Breaking Symmetry: Mutations Engineered into R67 Dihydrofolate Reductase, a D_2 Symmetric Homotetramer Possessing a Single Active Site Pore[†]

R. Derike Smiley,[‡] Lori G. Stinnett,[‡] Arnold M. Saxton,[§] and Elizabeth E. Howell*[,‡]

Department of Biochemistry and Cellular and Molecular Biology, University of Tennessee, Knoxville, Tennessee 37996-0840, and Department of Animal Science, University of Tennessee, Knoxville, Tennessee 37996-4500

Received August 19, 2002; Revised Manuscript Received November 4, 2002

ABSTRACT: R67 dihydrofolate reductase (DHFR) is an enzyme, encoded by an R-plasmid, that confers resistance to the antibacterial agent trimethoprim. This homotetramer possesses a single active site pore and exact 222 symmetry. The symmetry imposes constraints on the ability of the enzyme to optimize binding of the substrate, dihydrofolate (DHF), and the cofactor, NADPH, resulting in a "one site fits both ligands" approach. This approach allows formation of either a NADPH·NADPH, dihydrofolate·dihydrofolate, or NADPH·dihydrofolate complex. The first two complexes are nonproductive, while the third is the productive catalytic species. To break the symmetry of the active site, a tandem array of four R67 DHFR genes has been linked in frame, allowing individual manipulation of each gene copy. Various numbers and combinations of asymmetric Q67H mutations have been engineered into the tandem gene array. The Q67H mutation was chosen for investigation as it was previously found to tighten binding to both dihydrofolate and NADPH by ∼100-fold in homotetrameric R67 DHFR [Park, H., Bradrick, T. D., and Howell, E. E. (1997) *Protein Eng. 10*, 1415−1424]. Nonadditive effects on ligand binding are observed when one to four mutations are inserted, indicating either conformational changes in the protein or different cooperativity patterns in the ligand−ligand interactions. From steady state kinetics, addition of Q67H mutations does not drastically affect formation of the NADPH·dihydrofolate complex; however, a large energy difference between the productive and nonproductive complexes is no longer maintained. A role for Q67 in discriminating between these various states is proposed. Since theories of protein evolution suggest gene duplication followed by accumulation of mutations can lead to divergence of activity, this study is a first step toward asking if introduction of asymmetric mutations in the quadrupled R67 DHFR gene can lead to optimization of ligand binding sites.

Dihydrofolate reductase (DHFR)[1] reduces dihydrofolate (DHF) to tetrahydrofolate using the cofactor NADPH in a hydride transfer reaction. Tetrahydrofolate is essential for cell survival as it is a precursor for formation of thymidylate, methionine, purine nucleosides, and other intermediates in metabolism. The antibiotic trimethoprim has been used clinically as an inhibitor against *Escherichia coli* chromosomal DHFR. However, R67 DHFR, encoded by an R-plasmid, confers resistance to this antibiotic. This DHFR variant is not homologous in either genetic composition or structure to the chromosomally encoded enzyme (*2*, *3*).

Numerous observations lead to the hypothesis that R67 DHFR is a primitive enzyme. First, the active species is a homotetramer that possesses 222 symmetry as shown in Figure 1 [Protein Data Bank entry 1VIE (*3*)]. The single active site is a 25 Å pore that extends the length of the protein. As a consequence of the 222 symmetry, binding of DHF and NADPH to the pore results in formation of three different complexes [DHF·DHF, NADPH·NADPH, and DHF·NADPH (*4*)]. Only the ternary complex (DHF·NADPH) results in catalysis. For the latter complex, DHF occupies half the pore and cofactor the other half; the pteridine ring of DHF and the nicotinamide ring of NADPH encounter each other at the center of the pore where the reaction occurs (*5*). A drawback of the 222 symmetry is that binding to NADPH and DHF cannot be independently optimized. The enzyme appears to possess a binding "hot spot" that can accommodate (with some degree of overlap) both DHF and NADPH (*6*, *7*).

A second observation suggesting R67 DHFR is a primitive enzyme is that mutations typically have a large cumulative effect since one mutation per gene results in four mutations per active site. Mutations that tighten binding do not necessarily lead to enhanced catalytic efficiency as binding is concurrently tightened in all symmetry-related sites. This leads to substantial substrate and cofactor inhibition because

[†] This research was supported by NSF Grant MCB-9808302 (to E.E.H.).

* To whom correspondence should be addressed. Phone: (865) 974-4507. Fax: (865) 974-6306. E-mail: lzh@utk.edu.

[‡] Department of Biochemistry and Cellular and Molecular Biology.

[§] Department of Animal Science.

[1] Abbreviations: DHFR, dihydrofolate reductase; wt, wild-type; TMP, trimethoprim; DHF, dihydrofolate; $NADP^+$ and NADPH, oxidized and reduced nicotinamide adenine dinucleotide phosphate, respectively; NMNH, reduced nicotinamide mononucleotide; MTH buffer, 50 mM MES, 100 mM Tris, and 50 mM acetic acid polybuffer; ITC, isothermal titration calorimetry; CD, circular dichroism. Mutant enzymes containing amino acid substitutions are described by the wild-type residue and numbered position in the sequence followed by the amino acid substitution. For example, Q67H R67 DHFR describes the Gln67 → His mutant.

10.1021/bi026676j CCC: $22.00
Published on Web 12/07/2002

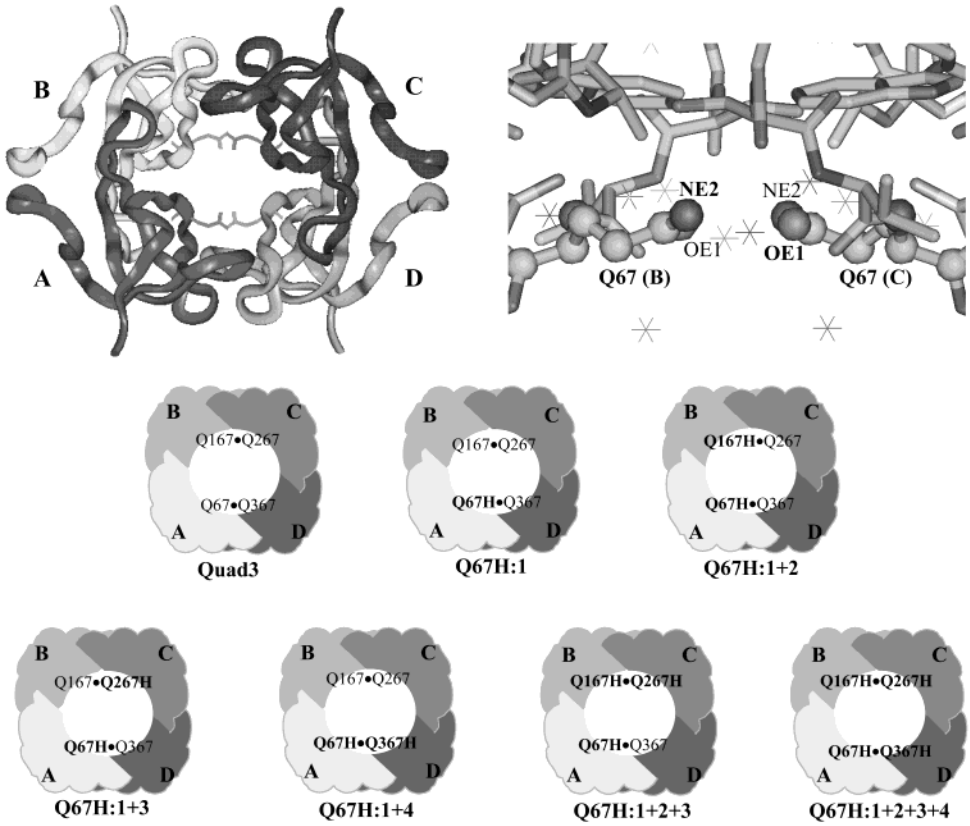

FIGURE 1: Ribbon structure of homotetrameric R67 DHFR (PDB entry 1VIE) (top left). Each monomer is shaded differently and labeled A, B, C, or D. While 1VIE has the monomer topology assigned as ABDC going clockwise, we have revised this to ABCD to minimize confusion in the four-gene copy construct. The single-active site pore occurs in the center of the structure. The Q67 side chains are highlighted; they appear at the top and bottom surfaces of the active site pore. An enlarged view of a pair of symmetry-related Q67 residues from the B and C subunits (top right). The Q67 residues are in the center of the image in ball-and-stick format and the NE2 and OE1 atoms labeled. Water molecules are given as stars. The active site pore is directly below the two glutamines. The bottom part of the figure is a cartoon representing the topologies of various asymmetric Q67H mutations. Quad3 is the parent structure that possesses covalent linkers between each monomer in homotetrameric (wt) R67 DHFR. Each monomer in wt R67 DHFR or respective domain in Quad3 is labeled A−D and shaded in different colors of gray. The side chains of the Q67 residues form pairwise H-bonding interactions at the ceiling and floor of the active site pore. The relative positions of the wt or mutant (bold) residues are shown for the various mutants.

of formation of the nonproductive complexes (DHF·DHF and NADPH·NADPH) (*1*, *4*).

A third observation is that R67 DHFR does not possess a general acid in its active site pore. Instead, it requires that the substrate be activated by protonation (*1*, *8*, *9*). In other words, catalysis becomes more rapid as the pH approaches the pK_a of N5 on DHF [2.59 (*10*)].

Introduction of asymmetric mutations should break the constraints imposed on R67 DHFR due to its 222 symmetry, leading to addition of functional groups or building substrate specificity. For the latter, mutations may be added to one half of the pore, leading to more specific binding of NADPH. Conversely, specificity may be built in the other half of the pore, allowing more precise binding of DHF. Construction of asymmetric mutations by mixing populations (e.g., wild-type and mutant R67 DHFRs) is limited by the pH-dependent dissociation of tetrameric R67 DHFR into dimers (*11*). Thus, any heterotetramers formed and isolated will readily dissociate and reassociate to a mixture of homo- and heterotetramers upon titration of His62 and its symmetry-related residues[2] at pH $\leq$8.

To construct asymmetric mutations in R67 DHFR, a gene oligomerization strategy is necessary. Therefore, Bradrick et al. (*12*) linked in frame four copies of the gene encoding the 78-amino acid monomer. The protein product of this tandem gene array is an active monomer with a mass 4 times greater than that of the wild-type (wt) monomer and that possesses the essential tertiary structure of the wt homotetramer. The linker between gene copies corresponds to the natural N-terminus. In this protein, residues are not numbered consecutively. Instead, residues 1−78 constitute the first domain (A), residues 101−178 the second domain (B), residues 201−278 the third domain (C), and residues 301−378 the fourth domain (D). The domains correspond to the monomers in wt R67 DHFR.

This paper describes the addition of asymmetric mutations to the tandem gene array. The Q67H substitution was initially chosen for analysis as it tightens binding to both NADPH and DHF in the context of the wt homotetramer (*1*). Glutamine 67 and its symmetry-related residues occur at the center of the active site pore. They form the "ceiling" and "floor" of the pore (Figure 1). Each Q67 residue hydrogen bonds with a symmetry-related Q67 residue at both dimer−

[2] The amino acids in the first monomer (A) are labeled 1−78, those in the second monomer (B) 101−178, those in the third monomer (C) 201−278, and those in the fourth monomer (D) 301−378. For brevity, when a single residue is mentioned, all four symmetry-related residues are implied. The monomer arrangement going clockwise in the crystal structure 1VIF is ABDC (*3*). To minimize confusion in the quadrupled gene construct, we have relabeled the monomers ABCD going clockwise.

dimer interfaces. Both of the hydrogen-bonded pairs extend into the active site, causing the pore radius to decrease near the middle. From the folate cocrystal structure, Q67 forms extensive van der Waals interactions with the pteridine ring of folate (*3*). Our recent computational docking studies using DOCK (docking based on van der Waals interactions) and SLIDE (docking based on hydrogen bond formation) predict interactions between Q67 and NMNH (reduced nicotinamide−ribose−P_i moiety of NADPH) (*6*). In these predicted interactions, Q67 may form a hydrogen bond to one of the ribose OH groups (O2′) through its NE2 group as well as van der Waals interactions with several atoms of the nicotinamide ring through its side chain. This ternary complex model proposes that Q67 serves a dual role in binding both folate/DHF and NADPH. The previously constructed Q67H mutant also supports this notion as it tightens binding to both NADPH and DHF by factors of 100- and 6000-fold, respectively (*1*). Binding affinity may be strengthened due to ring stacking interactions between the imidazole ring of histidine and the nicotinamide and/or pteridine rings of NADPH and DHF, respectively (*13*−*15*).

MATERIALS AND METHODS

Site-Directed Mutagenesis. A synthetic R67 DHFR gene, carried in pUC8, has previously been described (*16*). A tandem array of four R67 DHFR genes was previously constructed where the genes are linked in frame (*12*). The resulting protein, named Quad1, possesses a mass 4 times greater than that of the native R67 DHFR monomer. Mutations were introduced using the PCR-based protocol outlined in the Quickchange kit from Stratagene. DNA sequencing was performed by the University of Tennessee sequencing facility to confirm all constructs.

Protein Purification. E. coli STBLII cells [*F*$^-$*mcrA* Δ*(mcrB-hsdRMS-mrr) recA1 endA1 gyrA96 thi supE44 relA1* λ^-Δ*(lac-proAB)*; Gibco BRL] were used to maintain the tandem gene arrays as well as express the monomeric R67 DHFR and mutants (*17*). Cells were grown at 30 °C with shaking for approximately 60 h. The cells were lysed by sonication, and the crude protein extract was clarified with streptomycin sulfate and concentrated with 55% ammonium sulfate. The proteins were purified using the following chromatography columns: G-75 Sephadex size exclusion column, DEAE Fractogel column, Bio-Rad HighQ column, and FPLC HighQ column (*7*, *16*). The purity of the proteins was determined by SDS−PAGE.

Isothermal Titration Calorimetry. Binding affinities and the enthalpy associated with binding were monitored using isothermal titration calorimetry (ITC) as previously described (*1*, *4*). Briefly, measurements were carried out on a Microcal Omega Ultrasensitive Isothermal Titration Calorimeter equipped with a nanovoltmeter for improved sensitivity and connected to a circulating water bath for temperature control. The data were automatically collected by an IBM personal computer running DSCITC data acquisition software and were analyzed using Origin version 2.9 provided by the manufacturer. The design and operation of this instrument have been described by Wiseman et al. (*18*). Samples typically consisted of ∼90−100 μM protein in MTH buffer [50 mM MES, 100 mM Tris, 50 mM acetic acid, and 10 mM β-mercaptoethanol (pH 8)]. This buffer maintains a constant ionic strength from pH 4.5 to 9.5 (*19*). Measurements were performed at 28 °C. Ligand concentrations in the syringe were typically 20 times greater than the protein concentration. Addition of ligand to buffer only was performed to allow baseline corrections. Data describing NADPH or DHF binding were fit to an interacting sites model where the stoichiometry of ligand binding was set equal to 2. Data describing binding of $NADP^+$ were fit to a single-site model. Ternary complex data were obtained by titrating DHF into a 1:1 mixture of R67 DHFR and $NADP^+$ and were fit to a single-site model.

Scheme 1

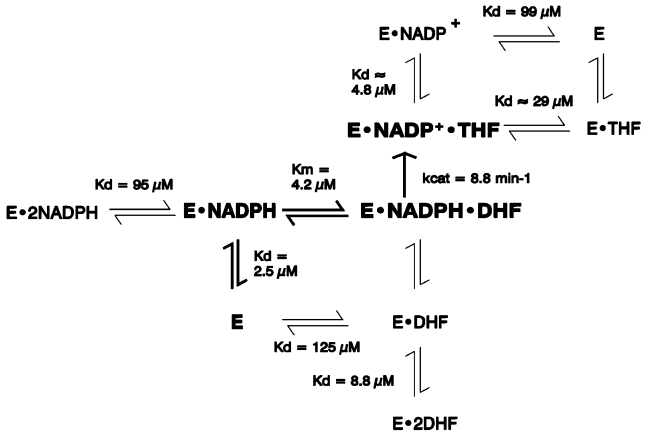

Steady State Kinetics. The kinetic behavior of each protein was monitored using a Perkin-Elmer λ3a spectrophotometer controlled by an IBM PS2 computer (*20*). The data were collected using the program UVSL3. Each experiment was conducted at 30 °C in MTH buffer. Four to five subsaturating concentrations of both DHF and NADPH were utilized to monitor activity. To calculate k_{cat} and K_m values for those variants displaying no or minimal substrate or cofactor inhibition, the data were fit globally to the nonlinear Michaelis−Menten equation describing bisubstrate kinetics using SAS version 8.2 (*21*; R. D. Smiley et al., manuscript in preparation). These values agree with the more traditional data analysis approach (*22*, *23*) where primary linear 1/[substrate] versus 1/velocity plots are followed by secondary plots, yielding kinetic parameters. To calculate k_{cat} and K_m values for those variants displaying substantial substrate and/or cofactor inhibition, the data were fit globally using SAS to a rate equation describing the R67 DHFR mechanism (*4*). The mechanism is shown in Scheme 1, and the corresponding rate equation is

$$v = \frac{k_{cat}[E_{total}][DHF][NADPH]}{[DHF][NADPH] + K_{m(DHF)}[NADPH] + K_{m(DHF)}K_{d1(NADPH)} + K_{m(NADPH)}[DHF] + K_{m(DHF)}[NADPH]^2/K_{d2(NADPH)} + K_{m(NADPH)}[DHF]^2/K_{d2(DHF)}} \quad (1)$$

where v is the velocity of the reaction, $[E_{total}]$, [DHF], and [NADPH] are the concentrations of the enzyme, substrate, and cofactor, respectively, and K_{d1} and K_{d2} are the first and second binding constants, respectively, for the specified ligands as measured by isothermal titration calorimetry (ITC).

In fitting these data sets, the K_d values obtained by isothermal titration calorimetry were used as constraints.

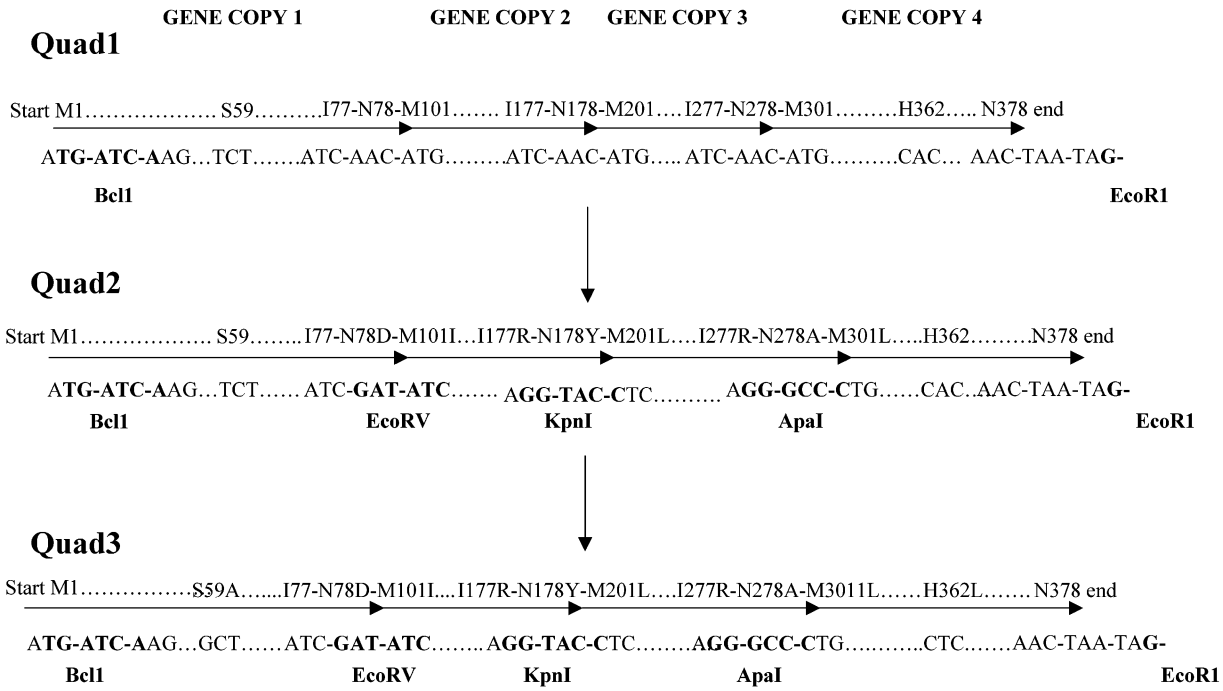

FIGURE 2: Flowchart for construction of the quadrupled R67 DHFR genes. The complete R67 DHFR gene sequence is given in ref *16*. Construction of the initial quadrupled gene, Quad1, is described in ref *12*. Each gene copy encoding a 78-amino acid monomer is denoted with a horizontal arrow. Partial DNA sequences with engineered unique restriction sites (in bold) are shown below the line, while the corresponding amino acids are given above the line. For Quad3, two additional mutations were added; gene copy 1 contains an S59A mutation, while gene copy 4 contains an H362L mutation (*29*).

Since three K_d values are entered explicitly with bounds allowing some minor variation, the fourth K_d is determined using a closed thermodynamic loop relationship [$K_{m(NADPH)} = K_{d1(NADPH)}K_{m(DHF)}/K_{d1(DHF)}$]. To keep any variation from funneling to the fourth K_d, a ratio of $K_{d1(NADPH)}$ to $K_{d1(DHF)}$ was sometimes used as a fixed parameter (again with bounds allowing some minor variation). In the fitting process, the input K_d values and the K_{d1} ratio were allowed to vary by 2−3-fold. If the 2−3-fold changes in K_d values gave better fits to the steady state kinetic data, then these K_d values were used to re-assess the ITC fits. All ITC refits remained within 90% confidence intervals.

Protein and ligand concentrations were determined spectrophotometrically. For all mutants, extinction coefficients were determined using the biuret assay (*24*). Ligand concentrations were determined using the following extinction coefficients: 28 000 L mol^{-1} cm^{-1} at 282 nm for DHF (*25*) and 6220 L mol^{-1} cm^{-1} at 340 nm for NADPH (*26*). The molar extinction coefficient used to assess DHFR reduction of DHF was 12 300 L mol^{-1} cm^{-1} (*27*).

RESULTS

Construction of an Altered Tandem Array. Direct mutagenesis of the quadrupled gene construct described by Bradrick et al. (*12*) did not allow control of either the number of mutations or their placement since each of the gene copies was identical. Therefore, a different mutagenesis strategy was devised. In this alternate approach, unique restriction sites were designed between the gene copies by mutagenesis of the 5′- and 3′-ends of each of the single-copy genes. This process resulted in four different single-R67 DHFR gene constructs. Introduction of an asymmetric mutation into the desired gene copy was next performed, and ligation of the resulting constructs allowed reconstruction of the quadrupled gene containing the desired asymmetric mutation(s).

The tandem array containing the restriction sites but no asymmetric mutations is named Quad2. Figure 2 shows a *Bcl*I site at the 5′-end of gene copy 1. An *Eco*RV site separates gene copies 1 and 2. A *Kpn*I site occurs between copies 2 and 3. An *Apa*I site divides gene copies 3 and 4. An *Eco*RI site is positioned at the 3′-end of gene copy 4. Introduction of the restriction sites into the gene creates several amino acid changes. The C-terminal wt R67 DHFR sequence is the Ile77-Asn78 pair; for direct connection to the second gene copy, the next residue would be Met101. However, for the construct that contains the *Eco*RV site, N78D and M101I mutations are present. For the construct that introduces the *Kpn*I site, I177R, N178Y, and M201L mutations occur. Last, for the *Apa*I restriction site, I277R, N278A, and M301L mutations are introduced. While these changes are not always conservative, a comparison of type II DHFR sequences indicates that the 26 N-terminal residues and the two C-terminal residues are not well conserved (*28*). Further, removal of the 16 N-terminal amino acids by chymotrypsin treatment does not affect enzyme activity (*16*).

From an examination of the homotetramer structure, it appears that formation of either an ABCD or an ABDC topology or a mixture of the two species in the quadrupled gene product is feasible. This option arises as the N-terminal Pro19 residues from the C and D monomers are equidistant (>45 Å) from the C-terminal N78 residue in the B monomer in the R67 DHFR crystal structure. These two symmetry-related Pro19 residues are ∼15 Å apart.[3] To constrain the

[3] The 17−18 N-terminal amino acids are disordered in the dimer structure (*53*), and when 16 N-terminal amino acids were cleaved off, the truncated protein crystallized as a tetramer (*3*).

various potential folding topologies to a single ABCD domain arrangement, we introduced an S59A mutation into gene copy 1 and an H362L mutation into gene copy 4. Individually, the S59A and H62L mutations destabilize the homotetramer, forming inactive dimers. However, 1:1 mixtures restore almost full activity, indicating they complement each other and form heterotetramers (*29*). The quadruple variant containing these mutations is named Quad3. All subsequent mutants described below use this as a "parent".

The final step in this process introduced Q67H mutations into Quad3. A single Q67H mutation was constructed in gene copy 1; single mutations in other gene copies were not constructed as the 222 symmetry of R67 DHFR predicts they will be equivalent. For double Q67H mutants, three nonequivalent constructs are possible. The first contains mutations in gene copies 1 and 2 (Q67H:1+2); the second contains Q67H mutations in gene copies 1 and 3 (Q67H:1+3), and the third contains Q67H mutations in gene copies 1 and 4 (Q67H:1+4). In the Q67H:1+2 construct, Q67H lies next to a wt Q67 residue at the floor as well as the ceiling of the pore and the mutations occur on the "left-hand" side of the pore. In the Q67H:1+3 construct, Q67H again lies next to a wt Q67 residue at the floor of the pore; however, the second Q67H mutation occurs "diagonally" across the pore on the ceiling. In the Q67H:1+4 construct, a Q67H pair should form at the floor of the active site pore while a wt Q67 pair should occur at the ceiling. From the symmetry, the Q67H:1+2 construct should be equivalent to a Q67H:3+4 construct; the Q67H:1+3 and Q67H:2+4 constructs should be equivalent as are the Q67H:1+4 and Q67H:2+3 constructs. Only one triple mutant, Q67H:1+2+3, was constructed as was a single quadruple mutant, Q67H:1+2+3+4. Figure 1 shows a cartoon of the mutant configurations.

Does the Quad3 Protein Mimic wt R67 DHFR? Prior to construction and evaluation of any asymmetric mutants, it was necessary to assess the effect of the mutations that added the unique restriction sites between gene copies, as well as the S59A and H362L mutations used to constrain possible folding topologies to the quadrupled gene product. To determine whether the Quad3 protein mimics wt R67 DHFR, steady state kinetics and isothermal titration calorimetry were utilized. Table 1 gives the k_{cat} and K_m values for wt R67 DHFR, the original Quad1 protein (*12*), as well as the Quad3 protein derived from this work. The k_{cat} and K_m values for Quad3 are similar to those of Quad1 and are within a factor of 2 of those of wt R67 DHFR, indicating the effects of the mutations are minor.

A comparison of ITC binding data for NADPH, DHF, and $NADP^+$ is given in Table 2. Again, the Quad3 protein mimics wt R67 DHFR reasonably well. The largest difference is an approximately 5-fold weaker binding of the first DHF molecule. However, the previously reported K_d values for DHF binding to wt DHFR were fit, including the first data point (*4*). In contrast, the values reported in this study do not use the first data point due to the variability associated with the first mixing event in the calorimeter. This difference in fitting explains an approximately 2-fold change in K_d. Any additional variance arises from differences between the Quad3 and wild-type proteins.

What Are the Effects of the Asymmetric Q67H Mutations? To assess the effects of the Q67H mutations on ligand binding, ITC was used to monitor binding to DHF, NADPH, and $NADP^+$ in various combinations. A representative titration is given in Figure 3. Data for all mutants except for the Q67H:1+2+3+4 variant were obtained. We find the data for this species are not readily reproducible as the protein solution often is turbid after the titration, indicating aggregation at high protein concentrations.

Table 3 gives the K_d and ΔH values associated with binding of $NADP^+$. Only one $NADP^+$ binds per R67 DHFR as compared to two NADPH molecules. This different stoichiometry is likely due to charge−charge repulsion between the positively charged nicotinamide rings in $NADP^+$. A trend noted is introduction of each successive Q67H mutation results in tighter binding of $NADP^+$ over a 7-fold range (with some variability for the different topologies of the double mutants). A generally linear relationship between the number of mutations and the K_d is consistent with no conformational changes upon binding and additive (independent) interactions between the Q67H residues (*30*). While a model does not exist for bound $NADP^+$, a model for bound,

Table 1: A Comparison of Steady State Kinetic Values at pH 7.0 for Numerous R67 DHFR Constructs

enzyme	k_{cat} (s^{-1})	$K_{m(NADPH)}$ (μM)	$K_{m(DHF)}$ (μM)	R^2 (%) (SAS)
wt R67 DHFR[a]	1.3	3.0	5.8	−
Quad1[b]	0.75	4.5	8.0	−
Quad3[c]	0.81 ± 0.02	4.4 ± 0.4	6.7 ± 0.4	90
Q67H:1[c]	0.23 ± 0.01	1.3 ± 0.1	3.6 ± 0.2	90
Q67H:1+2[d]	0.21 ± 0.01	0.28 ± 0.02	3.6 ± 0.3	89
Q67H:1+3[d]	0.23 ± 0.01	1.8 ± 0.1	11 ± 0.6	97
Q67H:1+4[d]	0.15 ± 0.01	0.95 ± 0.14	2.6 ± 0.5	84
Q67H:1+2+3[d]	0.090 ± 0.01	0.45 ± 0.06	7.5 ± 2.3	85%
Q67H:1+2+3+4[d]	0.10 ± 0.01	0.026 ± 0.004	0.13 ± 0.02	86
Q67H R67 DHFR (pH 8)[e]	0.022 ± 0.001	0.03 (calcd)	0.16 ± 0.005	−
Q67H R67 DHFR (pH 8)[f]	0.025 ± 0.001	0.014 ± 0.002	0.14 ± 0.01	91

[a] Values from ref *16*. [b] Values from ref *12*. [c] Global nonlinear fit to the Michaelis−Menten equation describing bisubstrate kinetics using SAS. [d] Global nonlinear fit (SAS) to a rate equation describing the R67 DHFR mechanism (eq 1) using ITC values as constraints. [e] Fit values from ref *1* using FITSIM. [f] Global nonlinear fit (SAS) to a rate equation describing the R67 DHFR mechanism (eq 1) using ITC values as constraints.

Table 2: A Comparison of wt R67 DHFR with Quad3 Using Isothermal Titration Calorimetry To Monitor Ligand Binding

complex	K_d (μM)	ΔH (cal/mol)	stoichiometry
wt R67 DHFR with NADPH[a]	5.0 ± 0.3	−8600 ± 200	1.56 ± 0.14
	48 ± 2	−5800 ± 2500	
Quad3 with NADPH	4.0 ± 0.3	−3000 ± 26	2[b]
	37.1 ± 3.0	−9400 ± 83	
wt R67 DHFR with DHF[a]	250 ± 50	−7900 ± 900	1.88 ± 0.1
	4.4 ± 0.7	−1400 ± 60	
Quad3 with DHF	46 ± 0.7	−8420 ± 110	2[b]
	2.0 ± 0.02	−3750 ± 39	
wt R67 DHFR with $NADP^+$[a]	99 ± 3	−7700 ± 500	0.99 ± 0.03
Quad3 with $NADP^+$	31.3 ± 1.3	−7000 ± 450	0.95 ± 0.02
wt R67 DHFR·$NADP^+$ with DHF[a]	4.8 ± 1.0	−11700 ± 300	1.22 ± 0.01
Quad3·$NADP^+$ with DHF	4.9 ± 0.1	−11500 ± 800	0.99 ± 0.01

[a] Results from ref *4*. Microscopic values (K_{d1} and K_{d2}) are reported. The statistical relationship between microscopic and macroscopic constants is $K_{d1} = {}^1/_2K_{d1}$ and $K_{d2} = 2K_{d2}$ (*52*). [b] The stoichiometry is set at 2 by choosing the two-interacting sites model in Origin, the software used by the ITC for fitting the data. Since the value is set, it is presented with no error.

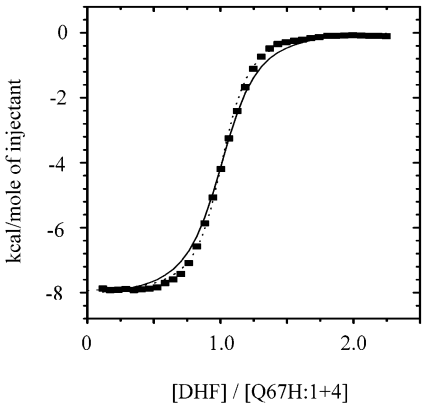

FIGURE 3: Isothermal titration calorimetry analysis of DHF binding to Q67H:1+4 DHFR. The protein concentration was 100 μM, and the data were fit using the two-interacting sites model (···). Best fit values are given in Table 4. To fit the steady state kinetic data (Table 1), the ITC values were allowed to vary up to 3-fold from the best fit values. In fitting of the kinetic data, the (microscopic) K_d values for DHF binding to Q67H:1+4 shifted to a K_{d1} of 2.12 and a K_{d2} of 106 μM. These involve a 2.3-fold increase and a 3-fold decrease from the K_d values given in Table 4. The refit is shown by the solid line.

Table 3: Binding of $NADP^+$ to the Various DHFR Species As Monitored by ITC at pH 8.0

complex	K_d (μM)	ΔH (cal/mol)	stoichiometry
Quad3 with $NADP^+$	31.3 ± 1.3	−7000 ± 450	0.95 ± 0.02
Q67H:1 with $NADP^+$	19.3 ± 1.9	−6500 ± 250	1.1 ± 0.03
Q67H:1+2 with $NADP^+$	13.1 ± 1.0	−7600 ± 240	1.1 ± 0.02
Q67H:1+3 with $NADP^+$	15.3 ± 1.4	−6300 ± 340	1.1 ± 0.01
Q67H:1+4 with $NADP^+$	11.2 ± 1.0	−13900 ± 520	1.0 ± 0.04
Q67H:1+2+3 with $NADP^+$	4.23 ± 0.3	−12200 ± 220	1.1 ± 0.05
Q67H R67 DHFR with $NADP^+$ [a]	3.4 ± 0.9	−9900 ± 500	0.70 ± 0.05

[a] Results from ref *1*.

reduced NMN has recently been generated by docking NMNH into R67 DHFR·FolI, where Fol1 is the productively bound pteridine ring in the crystal structure (*6*). In this model, the reduced nicotinamide moiety of NMN interacts with one pair of symmetry-related Q67 residues, while the pteridine ring of FolI interacts with the other pair of Q67 residues. One interpretation of the above ITC results suggests that bound $NADP^+$ interacts with at least three of the Q67 residues since successive addition of up to three mutations continues to tighten binding. This scenario would require $NADP^+$ to bridge both pairs of Q67 residues, a distance of ~11 Å (between carboxamide atoms). This interpretation suggests some alteration of the binding mode for $NADP^+$ with respect to that proposed for reduced NMN in a ternary complex. An alternate hypothesis is that when $NADP^+$ binds to either wt or Q67H R67 DHFRs, the binding constant reflects the statistical average of binding at each symmetry-related site. Since the sites are equivalent in the homotetramer, statistical averaging has no effect. However, when $NADP^+$ binds to an asymmetric mutant, for example, Q67H:1, there are several possible binding orientations; i.e., one symmetry pair of orientations would place the nicotinamide ring near a wt Q167−Q267 homopair, while a second pair of orientations would juxtapose the nicotinamide ring near the Q67H−Q367 heteropair. If the contribution of the Q67H residue to the overall binding constant is minor, the observed K_d may be an average value reflecting the

Table 4: Results of Binding Studies at pH 8.0 Using Isothermal Titration Calorimetry

complex	K_d (μM)	ΔH (cal/mol)	K_{d2}/K_{d1}
Quad3 with NADPH	4.0 ± 0.3	−3000 ± 26	9.3
	37.1 ± 3.0	−9400 ± 83	
Q67H:1 with NADPH	3.6 ± 0.8	−5800 ± 95	15
	53.5 ± 6.5	−9830 ± 160	
Q67H:1+2 with NADPH	2.7 ± 0.1	−5030 ± 28	5.6
	15.0 ± 0.4	−3530 ± 32	
Q67H:1+3 with NADPH	8.7 ± 0.5	−8650 ± 59	5.9
	51.1 ± 3.2	−5030 ± 91	
Q67H:1+4 with NADPH	17.7 ± 0.8	−8540 ± 100	0.91
	16.1 ± 0.5	−14000 ± 165	
Q67H:1+2+3 with NADPH	0.21 ± 0.01	−3740 ± 20	17
	3.5 ± 0.07	−2900 ± 75	
Q67H R67 DHFR with NADPH[a]	0.054 ± 0.016	−4800 ± 100	5.7
	0.31 ± 0.06	−2500 ± 400	
Quad3 with DHF	46 ± 0.7	−8420 ± 110	0.043
	2.0 ± 0.02	−3750 ± 39	
Q67H:1 with DHF	0.88 ± 0.06	−6340 ± 46	2.3
	2.0 ± 0.05	−5770 ± 74	
Q67H:1+2 with DHF	0.97 ± 0.04	−6250 ± 44	1.1
	1.1 ± 0.02	−5740 ± 45	
Q67H:1+3 with DHF	1.5 ± 0.05	−8500 ± 260	13
	20 ± 0.6	−1100 ± 33	
Q67H:1+4 with DHF	0.93 ± 0.03	−7340 ± 31	340
	320 ± 16	−3360 ± 23	
Q67H:1+2+3 with DHF	0.21 ± 0.1	−7350 ± 76	3.0
	0.64 ± 0.1	−7270 ± 82	
Q67H R67 DHFR with DHF[a]	0.040 ± 0.008	−8000 ± 100	identical sites

[a] Results from ref *1*.

contributions associated with binding at nonequivalent sites. As the number of Q67H mutations increases, this would lead to an overall decrease in the apparent K_d. This explanation seems more likely than the model in which $NADP^+$ interacts with at least three Q67H residues, although that cannot be ruled out.

A more complex relationship arises when the effects of the Q67H mutations on binding NADPH or DHF (binary conditions) are assessed. Table 4 gives the observed K_d and ΔH values. Several observations are apparent. First, for DHF binding, the addition of one Q67H mutation has a large, immediate effect on the first K_d value, while for NADPH binding, it takes three mutations to show any advance toward the tighter binding previously observed in the Q67H homotetramer (*1*). Second, the various double mutants exhibit different binding patterns, particularly for DHF, indicating they present different arrangements of the Q67H mutations. This implies that the Quad3 parent protein has been locked into a single topology (ABCD) and that the effect of two Q67H mutations is a function of how they are arranged with respect to each other. Third, the cooperativity between ligands (monitored by K_{d2}/K_{d1}) shows large variations, particularly for binding of DHF. These issues are discussed more fully below.

Since $NADP^+$ binding becomes progressively tighter with the successive addition of Q67H mutations, a straightforward result for binding of NADPH would have been a similar trend. Instead, addition of one Q67H mutation has a minimal effect on NADPH binding. Addition of two mutations has observable effects on binding, particularly for the Q67H:1+4 configuration, but tight binding is not observed. Only when three Q67H mutations are introduced does tighter binding begin to appear. While we would expect the Q67H:1+2+3+4 mutant to mimic the Q67H

Table 5: Ternary Complex Formation Monitored by ITC

complex	K_d (μM)	ΔH (cal/mol)	stoichiometry	$K_{d(DHF)ternary}/K_{d(NADP^+)binary}$
Quad3·$NADP^+$ with DHF	4.9 ± 0.1	−11500 ± 800	0.99 ± 0.01	0.16
Q67H:1·$NADP^+$ with DHF	2.2 ± 0.05	−11400 ± 940	1.0 ± 0.01	0.11
Q67H:1+2·$NADP^+$ with DHF	4.5 ± 0.1	−9400 ± 400	0.94 ± 0.01	0.34
Q67H:1+3·$NADP^+$ with DHF	4.8 ± 0.1	−9400 ± 600	1.07 ± 0.01	0.31
Q67H:1+4·$NADP^+$ with DHF	2.0 ± 0.05	−10000 ± 370	1.03 ± 0.01	0.18
Q67H:1+2+3·$NADP^+$ with DHF	6.6 ± 0.2	−8500 ± 590	1.01 ± 0.03	1.6
Q67H R67 DHFR·$NADP^+$ with DHF	6.7 ± 0.3	−9000 ± 450	0.82 ± 0.04	2.0

homotetramer and display 100-fold lower K_d values, we are unable to confirm this prediction due to protein aggregation.

The nonlinearity between the number of Q67H mutations and the corresponding NADPH K_d values suggests conformational changes may occur. These changes could describe altered interactions between either the wild-type Q67 and mutant Q67H residues and/or between the two ligands. The first alternative appears to be feasible as the Q67 residues occur very near the 222 symmetry operator and each Q67 residue interacts with its symmetry-related partner. Therefore, it would not be surprising if introduction of a Q67H mutation alters the position of the other member of the pair. Another possibility for explaining the binding data is that the cooperativity between the two NADPH molecules is altered. One measure of the interligand cooperativity is given by the K_{d2}/K_{d1} ratio. As seen in Table 4, this ratio varies from a low of 0.91 to a high of 17, depending on the number of mutations introduced as well as the positioning of the double mutants. We previously observed that this ratio varies less than 2-fold when studying NADPH binding to various homotetrameric R67 DHFR mutants [Q67H, I67L, and Y69F (*1*, *7*)]. This minimal variance of the K_{d2}/K_{d1} ratio was striking as the K_d values themselves varied over 3 orders of magnitude! From those studies, we concluded that interligand cooperativity is important in binding and catalysis in R67 DHFR and must be linked to the symmetry of the active site pore. Therefore, the data given in Table 4 are the first examples of varying levels of cooperativity associated with NADPH binding to R67 DHFR. We also find support for interligand cooperativity modulating the nonlinear effects of the asymmetric Q67H mutations on NADPH binding as the transition from a relatively linear relationship between the number of mutations and log K_d to a clearly nonlinear relationship occurs as the binding stoichiometry changes from one ($NADP^+$) to two (NADPH). This difference suggests the conformational changes could also arise from ligand−ligand interactions. The main differences between $NADP^+$ and NADPH are the positive charge and aromaticity of the nicotinamide ring in $NADP^+$.

In contrast to the results with NADPH described above, binding of DHF shows a clear effect upon addition of one Q67H mutation. Binding to the first DHF molecule is tightened by a factor of 52, suggesting a direct interaction between the Q67H mutation and DHF. The second K_d is also tight. Since the remaining residues are wt, this result suggests positive cooperativity remains between the two DHF molecules. Addition of two mutations shows varying results, depending on the configuration of the Q67H residues. For the Q67H:1+2 double mutant, both K_d values are relatively tight, suggesting either that each DHF is responding to the presence of the Q67H and Q167H mutations at the floor and ceiling of the pore or that positive cooperativity remains between the two DHF molecules. For the Q67H:1+3 and Q67H:1+4 double mutants, positive cooperativity between the DHF molecules clearly does not occur, and two possibilities can be envisioned to explain the binding pattern. Either the two DHF molecules now bind differently enough so that negative cooperativity occurs between them, or binding of the first DHF molecule is tight due to the presence of the Q67H mutations while binding of the second DHF molecule remains weak due to the interactions with the wt Q67 residues. For the latter, minimal to no DHF−DHF interactions would be expected. Alternatively, conformational changes associated with the mutations may be occurring as the K_ds for the Q67H:1 mutant are different from those for the Q67H:1+4 mutant. In these mutants, either one or two mutations occur at one interface while the other interface possesses only wt residues. If the second DHF binding event were responding only to the wt Q167−Q267 residues, then similar values would be expected for these K_ds. This is not observed. Finally, the introduction of three Q67H mutations also tightens binding to both DHF sites, although the effect is not as dramatic as for NADPH binding. That three mutations can continue to affect the first K_d also supports a model where conformational changes are occurring, either via altered interactions between the wild-type Q67 and mutant Q67H residues or between the two ligands. The latter model where ligand−ligand interactions influence the binding behavior remains feasible, as positive cooperativity between DHF molecules is observed in Quad3 while zero to negative cooperativity patterns are detected for the various Q67H asymmetric mutants.

Addition of DHF to the R67 DHFR·$NADP^+$ complex to form a ternary complex was additionally monitored by ITC methods. The K_d values are given in Table 5. Only minor variations are observed, indicating the affinity of DHF for the R67 DHFR·$NADP^+$ complex remains fairly constant throughout this series. To monitor interligand cooperativity between DHF and $NADP^+$, we have continued to use a ratio of the K_d for the second binding event divided by the K_d for the first binding event. In this case, the ratio is the K_d of DHF binding to the R67 DHFR·$NADP^+$ complex divided by the K_d for $NADP^+$ binding to R67 DHFR. The cooperativity values remain mostly constant and indicate positive cooperativity between the ligands, except for the Q67H:1+2+3 mutant, which indicates negligible or a slight negative cooperativity.

Steady State Kinetics of Asymmetric Mutants. The asymmetric mutants were additionally evaluated by steady state kinetic analysis. The values were readily determined for Q67H:1 using SAS to globally fit all the data to the Michaelis−Menten equation describing bisubstrate kinetics. The data and a three-dimensional (3D) representation of the

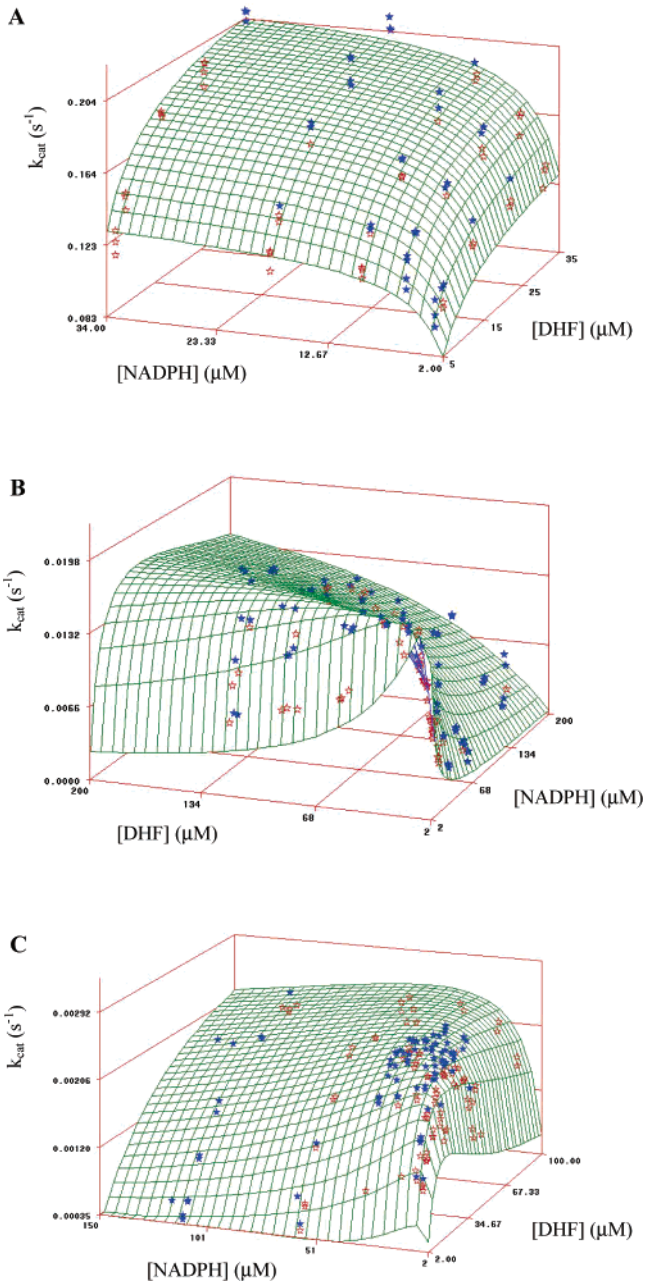

FIGURE 4: Steady state kinetic data for various R67 DHFRs. Panel A describes the Q67H:1 R67 DHFR, which was fit to the Michaelis−Menten equation describing bisubstrate kinetics using SAS. Data points above and below the calculated 3D plot are filled and empty stars, respectively. Panel B describes the Q67H homotetramer data (*1*). This representation reverses the axes for [DHF] and [NADPH] to accentuate a ridgeline of maximal activity. Nonlinear fitting was performed by SAS to eq 1, and Table 1 gives the best fit values. K_d values derived from ITC data were used as constraints in fitting with 2−3-fold variations accepted if the ITC data could be reasonably refit with these values. Panel C describes the Q67H:1+2 data as well as its accompanying 3D fit. The plots for the Q67H:1+3 and Q67H:1+4 double mutants are given as Supporting Information.

fit are shown in Figure 4A; best fit values are given in Table 1. Each grid line on the 3D plot corresponds to a constant first ligand concentration with varying second ligand concentrations (and vice versa). The K_m values both decrease ∼1.5-fold, and k_{cat} decreases 3-fold. These values agree with those determined by data linearization, followed by secondary replots (*22*, *23*).

Analysis of the kinetic data for the other mutants is less straightforward as they display various levels of substrate and cofactor inhibition. Therefore, a rate equation (eq 1) was derived for the mechanism describing inhibition associated with formation of the two nonproductive complexes (NADPH·NADPH and DHF·DHF) (*4*). The steady state kinetic data were then fit globally using SAS; the K_d values obtained by ITC were entered as constraints. Since the mechanism predicts formation of the NADPH·NADPH or DHF·DHF complexes as well as the productive NADPH·DHF complex, this fitting method requires data covering a wide range of substrate and/or cofactor "space" describing catalysis as well as inhibition. Therefore, between 130 and 370 data points were used in these fits.

Since global nonlinear SAS analysis of steady state kinetic data to a complicated rate equation is a new approach, we first confirmed its ability to fit the Q67H homotetramer data that had previously been analyzed with the computer program FITSIM (*1*, *31*). Our FITSIM analysis at that time indicated the Q67H homotetramer data could not be fit well without varying the ITC K_d values 2−3-fold. These alterations arose as NADPH was observed to be more inhibitory than DHF, even though the K_d values were similar. To fit the kinetic data, both NADPH K_d values were decreased 3-fold and both DHF K_d values were increased 2-fold. In this scenario, NADPH binds more tightly than DHF, providing more inhibition. SAS was able to identify this solution. In addition, SAS identified a second possibility where the cooperativity patterns were altered. In this solution, neither K_{d1} for NADPH or DHF was altered, but reduced negative cooperativity was proposed between the two NADPH molecules as well as the introduction of negative cooperativity between the two DHF molecules. In this second model, the NADPH·NADPH complex forms more easily than expected as its K_d values are closer, while it is harder to form the DHF·DHF complex as its K_d values are farther apart. A comparison of the correlation coefficient (R^2) for these two different fits supports the first SAS solution. Figure 4B shows the data overlaid on a 3D representation of the fit for the Q67H homotetramer. A good fit is observed with an R^2 value of 91%; best fit values are given in Table 1. This analysis clearly validates the SAS global fitting approach.

Analysis of the steady state kinetic data for the other asymmetric mutants was therefore performed using SAS. The data set for the Q67H:1+2 mutant and a 3D representation of the fit are given in Figure 4C. The data and 3D plots show substrate and/or cofactor inhibition at low second ligand concentrations. The fit values for this asymmetric mutant as well as the others are given in Table 1.

Each double mutant displays different kinetic behavior, indicating the various topologies generate different responses. The Q67H:1+2 double mutant displays obvious cofactor inhibition; its k_{cat} value decreases ∼3-fold, and K_m values decrease ∼16- and 2-fold for NADPH and DHF, respectively, leading to a 4-fold increase in $k_{cat}/K_{m(NADPH)}$. The next double mutant, Q67H:1+3, exhibits cofactor and substrate inhibition (particularly at a low second ligand concentration) as well as a ∼4-fold decrease in k_{cat}, a 2.5-fold decrease in $K_{m(NADPH)}$, and a slight (1.6-fold) *increase* in $K_{m(DHF)}$. The Q67H:1+4 double mutant displays no obvious substrate or cofactor inhibition and is readily saturated. While k_{cat} decreases ∼6-fold, $K_{m(NADPH)}$ decreases 5-fold, yielding a $k_{cat}/$

$K_{m(NADPH)}$ value approximately equal to that of Quad3. $K_{m(DHF)}$ decreases approximately 3-fold. The Q67H:1+2 double mutant is the most functional with respect to $k_{cat}/K_{m(NADPH)}$ values, while the Q67H:1+4 double mutant maintains its catalytic efficiency with no obvious substrate or cofactor inhibition. In fact, a fit of the Q67H:1+4 data to the bisubstrate kinetics equation provides very similar fit values.

The triple mutant shows more obvious NADPH and DHF inhibition, and the corresponding fit indicates a further decrease in k_{cat}, and K_m values that remain within the range of the double mutants. The quadruple mutant displays increasing levels of NADPH and DHF inhibition, similar to that of the Q67H homotetramer (*1*). The data set for the Q67H:1+2+3+4 mutant was fit using the ITC K_d values measured for the Q67H homotetramer as constraints; the values were allowed to deviate up to 4-fold (within the range of the Q67H:1+2+3 mutant). For the quadruple mutant, k_{cat} decreases 8-fold with respect to that of Quad3, while $K_{m(NADPH)}$ decreases 170-fold and $K_{m(DHF)}$ 48-fold. This leads to a 21-fold increase in $k_{cat}/K_{m(NADPH)}$ which is accompanied by tighter binding of NADPH and DHF at symmetry-related sites, resulting in severe cofactor and/or substrate inhibition. The similarity between kinetic values suggests the Q67H:1+2+3+4 quadruple mutant mimics the Q67H homotetramer reasonably well.

To deal with the fitting of the kinetic data, SAS varied the K_d constraints by various combinations of two approaches: either by maintaining the cooperativity but changing the overall K_d values 2−3-fold (the Q67H:1+2+3, Q67H:1+2+3+4, and Q67H homotetramer data sets) or by altering the cooperativity between ligands. For example, in the Q67H:1+2 data set, negative cooperativity between NADPH molecules was weakened (8-fold) while negative cooperativity between the two DHF molecules was enhanced (2-fold). For the Q67H:1+3 data set, cooperativity between NADPH molecules was maintained while binding was strengthened (3-fold), but the negative cooperativity between DHF molecules was enhanced (6-fold). For the Q67H:1+4 data set, negative cooperativity was enhanced between NADPH molecules (9-fold, i.e., a 3-fold tighter binding of the first NADPH and a 3-fold weaker binding of the second NADPH), while negative cooperativity was weakened between DHF molecules (7-fold). Fitting the kinetic data with reasonable R^2 values required changes in the ITC constraints. Changes of 2−3-fold in K_d values were tolerated by the ITC refits reasonably well.

Effects of the Mutations on Protein Structure. To confirm that all the Quad3 protein variants are monomeric, gel filtration studies were performed to assess how the oligomeric state varies as a function of pH. All measurements confirm the protein is a monomer at both pH 5 and 8 (data not shown). We further assessed the level of structural change by monitoring the equilibrium between "closed" and "open" forms of the quadrupled gene product (which correspond to the tetrameric and dimeric forms in wt R67 DHFR) using protein fluorescence. This titration monitors the pK_a of the symmetry-related H62 residues (of which three remain in Quad3 as it contains a complementing S59A and H362L pair) by the fluorescence of nearby W38 residues (*11*, *12*). The behavior of Quad3 continues to mimic that of Quad1, while the Q67H mutations slightly destabilize the closed structure (see the table in the Supporting Information). All proteins are in the active (closed) form for activity measurements at pH 7 and ITC measurements at pH 8.

Because the nonadditive nature of the kinetic and binding data suggests either a conformational change in the protein or alterations in the ligand−ligand interactions, we assessed the effect of the mutations on protein structure by CD measurements. There is some variation in the CD signal (not shown). The largest change is observed in the Q67H:1+2+3+4 mutant; however, this signal change correlates with that previously seen for the Q67H homotetramer (*1*). While these spectral changes may reflect some degree of conformational change, they also could arise from the proximity of the Q67H mutation to W38 (∼3.7−4 Å), as Woody (*32*) indicates aromatic side changes can make detectable contributions to the far-UV CD signal.

DISCUSSION

The Q67H homotetramer has been observed to bind both NADPH and DHF more tightly (≥100-fold) than wild-type R67 DHFR (*1*). Linked to this behavior was a 6.8-fold decrease in k_{cat}, resulting in a 3.6-fold enhancement in $k_{cat}/K_{m(NADPH)}$. However, the ability of the Q67H mutant to reach its transition state was compromised by tighter binding of a second identical ligand at a symmetry-related site, leading to substantial cofactor and substrate inhibition. Therefore the symmetry in the active site pore imposes a balance between catalysis and inhibition. Introduction of asymmetric mutations was pursued to determine if tight binding of the transition state could be uncoupled from inhibition. We reasoned if addition of one or two mutations was sufficient to tighten binding at one binding surface, the remaining wild-type residues at the other binding surface might not invoke tight binding and inhibition could be blocked. We address these linked issues by discussing the interligand cooperativities as measured by ITC, followed by steady state kinetic analysis.

What Is the Role of Interligand Cooperativity in R67 DHFR? Our previous mutations at Q67, I68, and Y69 in the context of the homotetramer (i.e., four mutations per active site pore) show minimal to no changes in NADPH cooperativity over a 1000-fold change in binding affinity (*1*, *7*). We previously interpreted this result to indicate either changes in affinity occur at all symmetry-related sites leading to similar effects or interligand cooperativity is quite important in ligand binding and catalysis. This is the first case where significant changes in NADPH cooperativities have been observed in R67 DHFR. Essentially no cooperativity between two NADPH molecules is observed for the Q67H:1+4 double mutant, while a 17-fold difference exists between the K_d values for the Q67H:1+2+3 mutant. Further, the DHF−DHF interaction varies dramatically with Quad3 displaying positive cooperativity and the Q67H:1+4 mutant possessing either independent sites or negative cooperativity. The range of K_{d2}/K_{d1} for DHF binding varies from 0.043 to 340, a 7900-fold effect. Formation of the $NADP^+$·DHF ternary complex also shows effects over a 10-fold range. That the cooperativity between $NADP^+$ and DHF is least affected suggests a preference for the heteroligand complex, a catalytic advantage that R67 DHFR utilizes.

Figure 5 compares the cooperativities between the various two-ligand complexes, where cooperativity measures the K_d

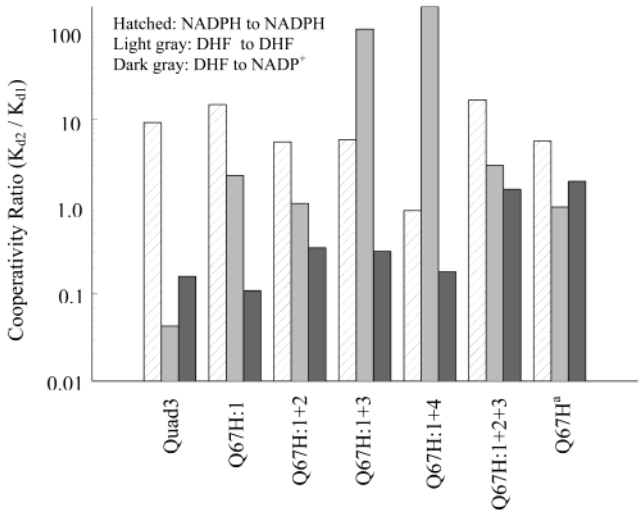

FIGURE 5: Bar graph comparing cooperativity ratios for the various protein constructs. The cooperativity between the first and second bound NADPH molecules (hatched bar) is described by K_{d2}/K_{d1} (see Table 4). The cooperativity between the DHF molecules (light gray bar) is given by K_{d2}/K_{d1} (see Table 4). The cooperativity between $NADP^+$ and DHF (dark gray bar) is given by $K_{d(DHF)ternary}/K_{d(NADP^+)binary}$ (see Table 5). Data for the Q67H homotetramer were from ref *1*.

for binding of the second ligand divided by the K_d for binding the first ligand. Quad3 shows negative cooperativity between the two NADPH molecules, positive cooperativity between the two DHF molecules, and positive cooperativity between $NADP^+$ and DHF, i.e., ternary complex formation. To increase the catalytic efficiency, these traits should be enhanced or, alternately, the strong positive cooperativity between the two DHF molecules could theoretically be replaced by a strong negative cooperativity. Negative cooperativity patterns are observed for the Q67H:1+3 and Q67H:1+4 double mutants. How does this translate into steady state kinetic behavior? Also, the cooperativity ratios for the triple mutant show the most convergence. Does this correlate with an inability to discriminate between the various complexes?

Patterns of Steady State Kinetic Behavior. As discussed above, two issues arise in R67 DHFR catalysis. The first is stabilization of the productive ternary complex leading to the transition state. The second issue arising from the 222 symmetry of the active site pore is competing formation of inhibitory complexes. To express this in an energy landscape perspective, R67 DHFR binds three complexes (DHF·DHF, NADPH·NADPH, and NADPH·DHF). To enhance catalysis, R67 DHFR can either stabilize the NADPH·DHF complex or destabilize the NADPH·NADPH and DHF·DHF complexes. The latter approach is termed negative design (*33*−*35*).

This second issue arises when considering the steady state kinetic behavior of the Q67H mutation series. Increasing levels of substrate and/or cofactor inhibition are noted as the number of mutations increases, with Quad3 showing no evidence of inhibition at the assay concentrations that were used (6−121 μM NADPH and 4−112 μM DHF), the double mutants exhibiting zero to moderate levels of inhibition and the triple and quadruple mutants displaying severe inhibition. Quad3 appears to have evolved a reasonable binding surface that achieves a low-free energy state for the NADPH·DHF complex coupled with a large free energy difference between productive and nonproductive complexes. While addition of Q67H mutations slightly alters binding to the NADPH·DHF complex, a large energy difference between the NADPH·DHF complex and the NADPH·NADPH and DHF·DHF states is no longer maintained, resulting in increasing levels of inhibition.

The competition between the three ligation states can clearly be seen in the 3D plots describing bisubstrate kinetics. We begin this discussion considering the simple 3D plot for Q67H:1 which shows no inhibition at the concentrations that are shown (Figure 4A). Hyperbolic [two-dimensional (2D)] plots can be seen on all four vertical edges of the cube, and a plateau can be seen at the upper back corner of the cube as Q67H:1 approaches its k_{cat} value (0.23 s^{-1}) at a 1:1 ratio of DHF to NADPH. In contrast, the Q67H homotetramer (Figure 4B) shows that at low levels of DHF, addition of NADPH is inhibitory due to the formation of the NADPH·NADPH complex (2D plot on the right face of the cube). At high NADPH concentrations, addition of DHF displays hyperbolic kinetics (back face of the cube), but since the enzyme is strongly inhibited due to formation of the NADPH·NADPH complex, the only possibility is for the activity to rise. This curve does not reach k_{cat} (0.025 s^{-1}) as there is always some level of inhibition present. At low levels of NADPH, addition of DHF is inhibitory due to formation of the DHF·DHF complex (front face of the cube). At high DHF concentrations, addition of NADPH shows initial hyperbolic kinetics followed by inhibition (left face of the cube). Again, since the enzyme is strongly inhibited under these high-DHF conditions, the activity can only increase. The rate increases until the NADPH concentration becomes sufficiently high to be inhibitory and the NADPH·NADPH complex forms (back corner of the cube). The k_{cat} is never reached anywhere on the surface of this 3D plot. A "ridgeline" that describes maximal activity can be clearly seen. The ridgeline appears to correspond to a 1:1 ratio of DHF to NADPH, modified by the relative inhibitory capacities of the DHF·DHF to NADPH·NADPH complexes.

Another way to consider the kinetic results is that the cooperativity patterns for the various double mutants vary substantially, yet k_{cat} is barely affected. This behavior indicates the cooperativity associated with reaching the productive ternary complex state has not changed dramatically (see Table 5). What has changed is the ability of the NADPH·NADPH and/or DHF·DHF complexes to compete favorably for formation. When these dead-end complexes readily form, the ability of the mutant enzyme to reach k_{cat} decreases. This is clearly shown in Figure 4B for the Q67H homotetramer.

Role of Q67H in Interligand Interactions? Gene duplication followed by divergence is commonly proposed as a mechanism of enzyme evolution. In this study, we quadrupled the gene for R67 DHFR and introduced various combinations of Q67H mutations. While addition of the Q67H mutation in the homotetramer tightens binding to both ligands by a factor of 100, this effect does not appear in an additive fashion as increasing numbers of Q67H mutations are added asymmetrically to the quadrupled gene product. This study of gradually breaking the symmetry of the binding surface suggests one consequence of the symmetry is overdetermination of the binding interactions, particularly for the heteroligand complex. While addition of a single

Q67H mutation might be expected to provide one tight binding interaction that would enhance binding, we find introduction of a single mutation has minimal effects on catalysis. For example, while similar K_d values for binding two DHF molecules lead to the prediction of DHF inhibition in the Q67H:1 variant, none is observed. This suggests the remaining wt sites maintain their function and are strongly preferred during catalysis. If a pair of Q67 residues need to interact to provide one tight binding surface, then the Q67H: 1+4 double mutant would be expected to enhance binding as these mutations form a pairwise interaction. This double mutant shows larger effects on ligand binding, but minimal effects on k_{cat}, again suggesting an overdetermination of the binding sites with a preference for wt sites. As three or four mutations are added, stronger effects on catalysis are noted, with the ability of the enzyme to discriminate between the productive ternary complex and nonproductive homoligand complexes becoming compromised. While the 222 symmetry in R67 DHFR imposes numerous deleterious effects on binding and catalysis, overdetermination of the binding site suggests an evolutionary advantage for symmetry as asymmetric mutations are introduced.

An alternate, but linked, point of view suggests that while protein interactions are important, the symmetry in R67 DHFR has selected for a strong influence arising from heteroligand interactions. While the $NADP^+$·DHF complex is not the catalytic species, it provides a reasonable mimic. The ternary complex K_d values (Table 5) as well as the k_{cat} values (Table 1) suggest that the heteroligand interactions are maintained (for the most part) in all the asymmetric mutants and perhaps drive binding. Additional support for this point of view comes from an *ab initio* quantum mechanical calculation that predicts the *endo* transition state (where the nicotinamide ring overlaps the more bulky side of the pteridine ring) is 2−8 kcal/mol more stable than the *exo* transition state [with minimal overlap of the pteridine and nicotinamide rings (*36*, *37*)]. Interligand NOE NMR data also favor R67 DHFR using an *endo* transition state (*5*) as do our docking studies focused on generating a ternary complex model (*6*). Some degree of ring stacking may allow R67 DHFR to partition binding toward the ternary complex.

While Q67 appears to play a minimal role in formation of the NADPH·DHF complex, it appears to be more active in discriminating against formation of the NADPH·NADPH and DHF·DHF complexes. Describing how the Q67H mutations affect the two-DHF and two-NADPH complexes will require better models of these complexes. From the crystal structure of the R67 DHFR·folate·folate complex, the N1- and N3-containing rings of the pteridine moieties overlap (*3*). More recent studies monitoring interligand NOEs (ILOEs) in R67 DHFR (*5*) describe a folate·2-deamino-2-methyl-5,8-dideazafolate complex with a similar overlap of the N1- and N3-containing rings of the pteridines. In contrast, no structural information about the NADPH·NADPH complex is available. How does R67 DHFR differentiate between these various complexes? Perhaps a clue comes from our ITC studies that measure the enthalpies associated with ligand binding.

Figure 6 shows a plot of ΔH versus $T\Delta S$ for the various complexes. Binding can be altered in mutant enzymes by different degrees of hydrogen bonding and van der Waals contacts which in turn can alter the degrees of freedom of

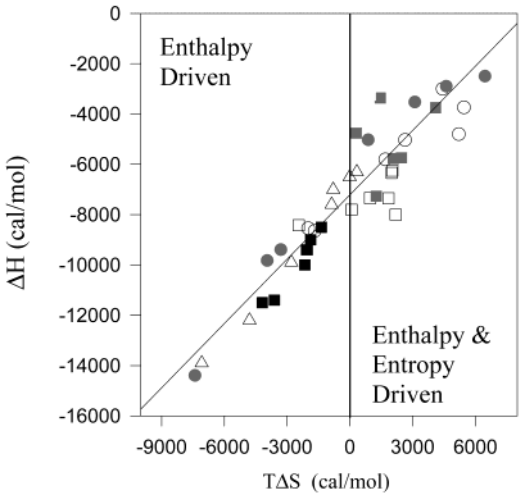

FIGURE 6: Plot of entropy ($T\Delta S$) vs enthalpy (ΔH) for various mutants and ligands. Binding data from Quad3, Q67H:1, Q67H: 1+2, Q67H:1+3, Q67H:1+4, Q67H:1+2+3, and the Q67H homotetramer proteins (*1*) are included. Values for binding the first and second NADPH molecules are given by empty and gray circles, respectively. Values for binding the first and second DHF molecules are given by empty and gray squares, respectively. Values for binding $NADP^+$ are shown with triangles, and values for DHF binding to the R67 DHFR·$NADP^+$ complex are given with black squares. The slope of the line is 0.85, and the correlation coefficient is 0.87. A plot of ΔH vs ΔG shows no correlation (not shown).

the ligand and amino acid side chain (*38*, *39*). The former would affect ΔH and the latter $T\Delta S$. Solvent reorganization may be involved in the effects of different ligands and mutant enzymes on ΔH and $T\Delta S$ (*40*, *41*). Finally, any proton exchange between enzyme and buffer to which ligand binding may be coupled could also be perturbed by use of a different mutant and result in a concomitant change in the thermodynamics of ligand binding. With these caveats in mind, it is worth noting that all the asymmetric proteins in this series show binding of DHF to the R67 DHFR·$NADP^+$ complex is enthalpy-driven. When trends within an enzyme variant are considered, most of the binary binding interactions for Quad3 are enthalpy-driven as are those for the Q67H: 1+4 mutant. In contrast, binding in the other mutants is driven by both thermodynamic components (enthalpy and entropy).

Calderone and Williams (*42*) suggest structural tightness displays a positive correlation with the exothermicity of the binding interaction. Maintaining enthalpy-driven formation of the ternary complex in these Q67H asymmetric mutants suggests a strong role for enthalpy in catalysis. Our studies support recent reports of catalytic function that suggest a strong role for enthalpy (*43*−*51*).

To conclude, formation of the R67 DHFR·DHF·$NADP^+$ ternary complex is enthalpy-driven, and introduction of Q67H mutations does not drastically affect its formation. This result suggests a strong role for interligand ($NADP^+$ to DHF) interactions in complex formation (presumably, interligand interactions would be important in the NADPH·DHF complex as well). Further, addition of increasing numbers of Q67H mutations results in the inability of the enzyme to discriminate between the productive and nonproductive complexes. These results support a role for Q67 in minimizing formation of the NADPH·NADPH and DHF·DHF complexes.

The Q67H:1+4 double mutant remains an interesting mutant as it displays minimal NADPH and DHF inhibition and it tightly binds the productive ternary complex (ΔH in Table 5) as well as maintains its $k_{cat}/K_{m(NADPH)}$ value. This mutant may serve as a stepping stone for addition of other asymmetric mutations, leading to the design of an alternate active site constellation with half the pore preferentially binding DHF and the other half binding NADPH. Further, we anticipate addition of asymmetric mutations at positions further away from the 222 symmetry operator will allow ready analysis of their effects as these substitutions will not be involved in the pairwise interactions that occur at the unusual position at the center of the pore.

ACKNOWLEDGMENT

We thank Cynthia Peterson for helpful advice and comments on the manuscript.

SUPPORTING INFORMATION AVAILABLE

Steady state kinetic data for Q67H:1+3 and Q67H:1+4 R67 DHFRs (Figure A), a series of fluorescence titration curves monitoring the equilibrium between open and closed forms of Quad3 and its mutants (Figure B), and a table of pK_a values describing titration of Quad3 variants from a closed to an open form as monitored by fluorescence. This material is available free of charge via the Internet at http://pubs.acs.org.

REFERENCES

1. Park, H., Bradrick, T. D., and Howell, E. E. (1997) *Protein Eng. 10*, 1415−1424.
2. Brisson, N., and Hohn, T. (1984) *Gene 28*, 271−275.
3. Narayana, N., Matthews, D. A., Howell, E. E., and Xuong, N. H. (1995) *Nat. Struct. Biol. 2*, 1018−1025.
4. Bradrick, T. D., Beechem, J. M., and Howell, E. E. (1996) *Biochemistry 35*, 11414−11424.
5. Li, D., Levy, L. A., Gabel, S. A., Lebetkin, M. S., DeRose, E. F., Wall, M. J., Howell, E. E., and London, R. E. (2001) *Biochemistry 40*, 4242−4252.
6. Howell, E. E., Shukla, U., Hicks, S. N., Smiley, R. D., Kuhn, L. A., and Zavodszky, M. I. (2001) *J. Appl. Comput.-Aided Mol. Des. 15*, 1035−1052.
7. Strader, M. B., Smiley, R. D., Stinnett, L., VerBerkmoes, N. C., and Howell, E. E. (2001) *Biochemistry 40*, 11344−11352.
8. Park, H., Zhuang, P., Nichols, R., and Howell, E. E. (1997) *J. Biol. Chem. 272*, 2252−2258.
9. Deng, H., Callender, R., and Howell, E. E. (2001) *J. Biol. Chem. 276*, 48956−48960.
10. Maharaj, G., Selinsky, B. S., Appleman, J. R., Perlman, M., London, R. E., and Blakley, R. L. (1990) *Biochemistry 29*, 4554−4560.
11. Nichols, R., Weaver, C. D., Eisenstein, E., Blakley, R. L., Huang, T.-H., Huang, F.-Y., and Howell, E. E. (1993) *Biochemistry 32*, 1695−1706.
12. Bradrick, T. D., Shattuck, C., Strader, M. B., Wicker, C., Eisenstein, E., and Howell, E. E. (1996b) *J. Biol. Chem. 271*, 28031−28037.
13. Brocchierei, L., and Karlin, S. (1994) *Proc. Natl. Acad. Sci. U.S.A. 91*, 9297−9301.
14. Hakoshima, T.-I., Itoh, T., Tomita, K.-I., Goda, K., Nishikawa, S., Morioka, H., Uesugi, S.-I., Ohtsuka, E., and Ihehara, M. (1992) *J. Mol. Biol. 223*, 1013−1028.
15. Sapse, A. M., Schweitzer, B. S., Diker, A. P., Bertino, J. R., and Frecer, V. (1992) *Int. J. Pept. Res. 39*, 18−23.
16. Reece, L. J., Nichols, R., Ogden, R. C., and Howell, E. E. (1991) *Biochemistry 30*, 10895−10904.
17. Strader, M. B., and Howell, E. E. (1997) *Gibco-BRL Focus 19*, 24−25.
18. Wiseman, T., Williston, S., Brandts, J. F., and Lin, L.-N. (1989) *Anal. Biochem. 179*, 131−137.
19. Ellis, K. J., and Morrison, J. F. (1982) *Methods Enzymol. 87*, 405−426.
20. Howell, E. E., Warren, M. S., Booth, C. L. J., Villafranca, J. E., and Kraut, J. (1987) *Biochemistry 26*, 8591−8598.
21. Segel, I. H. (1975) *Enzyme Kinetics*, John Wiley and Sons, New York.
22. Cleland, W. W. (1963) *Biochim. Biophs. Acta 67*, 104−137.
23. Smiley, R. D., Hicks, S. N., Stinnett, L. G., Howell, E. E., and Saxton, A. M. (2002) *Anal. Biochem. 301*, 153−156.
24. Gornall, A. G., Bardawill, C. J., and David, M. M. (1949) *J. Biol. Chem. 177*, 751−766.
25. Blakley, R. L. (1960) *Nature 188*, 231−232.
26. Horecker, B. L., and Kornberg, A. (1948) *J. Biol. Chem. 175*, 325−390.
27. Baccanari, D., Phillips, A., Smith, S., Sinski, D., and Burchall, J. (1975) *Biochemistry 14*, 5267−5273.
28. Flensburg, J., and Steen, R. (1986) *Nucleic Acids Res. 14*, 5933.
29. Dam, J., Rose, T., Goldberg, M. E., and Blondel, A. (2000) *J. Mol. Biol. 302*, 235−250.
30. Wells, J. A. (1990) *Biochemistry 29*, 8509−8517.
31. Zimmerle, C. T., and Frieden, C. (1989) *Biochem. J. 258*, 381−387.
32. Woody, R. W. (1995) *Methods Enzymol. 246*, 34−71.
33. Richardson, J. S., and Richardson, D. C. (2002) *Proc. Natl. Acad. Sci. U.S.A. 99*, 2754−2759.
34. Hellinga, H. (1998) *J. Am. Chem. Soc. 120*, 10055−10066.
35. Hecht, M. H., Richardson, J. S., Richardson, D. C., and Ogden, R. C. (1990) *Science 249*, 884−891.
36. Andres, J., Moliner, V., Safont, V. S., Domingo, L. R., Picher, M. T., and Krechl, J. (1996) *Bioorg. Chem. 24*, 10−18.
37. Castillo, R., Andres, J., and Moliner, V. (1999) *J. Am. Chem. Soc. 121*, 12140−12147.
38. Gilli, P., Ferretti, V., Gilli, G., and Borea, P. A. (1994) *J. Phys. Chem. 98*, 1515−1518.
39. Dunitz, J. D. (1995) *Chem. Biol. 2*, 709−712.
40. Chervenak, M. C., and Toone, E. J. (1994) *J. Am. Chem. Soc. 116*, 10533−10539.
41. Grunwald, E., and Steel, C. (1995) *J. Am. Chem. Soc. 117*, 5687−5692.
42. Calderone, C. T., and Williams, D. H. (2001) *J. Am. Chem. Soc. 123*, 6262−6267.
43. Bruice, T. C. (2002) *Acc. Chem. Res. 35*, 139−148.
44. Bruice, T. C., and Benkovic, S. J. (2000) *Biochemistry 39*, 6267−6274.
45. Bruice, T. C., and Lightstone, F. C. (1999) *Acc. Chem. Res. 32*, 127−136.
46. Shurki, A., Strajbl, M., Villa, J., and Warshel, A. (2002) *J. Am. Chem. Soc. 124*, 4097−4107.
47. Snider, M. J., Gaunitz, S., Ridgway, C., Short, S. A., and Wolfenden, R. (2000) *Biochemistry 39*, 9746−9743.
48. Snider, M. J., Lazarevic, D., and Wolfenden, R. (2002) *Biochemistry 41*, 3925−3930.
49. Villa, J., Strajbl, M., Glennon, T. M., Sham, Y. Y., Chu, Z. T., and Warshel, A. (2000) *Proc. Natl. Acad. Sci. U.S.A. 97*, 11899−11904.
50. Wolfenden, R., Snider, M., Ridgway, C., and Miller, B. (1999) *J. Am. Chem. Soc. 121*, 7419−7420.
51. Wolfenden, R., and Snider, M. (2001) *Acc. Chem. Res. 34*, 938−945.
52. Cantor, C. R., and Schimmel, P. R. (1980) Biophysical Chemistry Part II, *The Behavior of Biological Macromolecules*, W. H. Freeman & Co., San Francisco.
53. Matthews, D. A., Smith, S. L., Baccanari, D. P., Burchall, J. J., Oatley, S. J., and Kraut, J. (1986) *Biochemistry 25*, 4194−4204.

BI026676J